Strong Light-Matter Interactions in Single Open Plasmonic Nanocavities at the Quantum Optics Limit

Renming Liu,[1] Zhang-Kai Zhou,[1] Yi-Cong Yu,[2] Tengwei Zhang,[1] Hao Wang,[3] Guanghui Liu,[1] Yuming Wei,[1] Huanjun Chen,[1] and Xue-Hua Wang[1,*]

[1]*State Key Laboratory of Optoelectronic Materials and Technologies, School of Physics, Sun Yat-sen University, Guangzhou 510275, China*

[2]*School of Physics and Optoelectronic Engineering, Foshan University, Foshan 528000, China*

[3]*Guangdong Province Key Laboratory of Display Material and Technology, Sun Yat-sen University, Guangzhou 510275, China*

(Received 28 July 2016; published 8 June 2017)

Reaching the quantum optics limit of strong light-matter interactions between a single exciton and a plasmon mode is highly desirable, because it opens up possibilities to explore room-temperature quantum devices operating at the single-photon level. However, two challenges severely hinder the realization of this limit: the integration of single-exciton emitters with plasmonic nanostructures and making the coupling strength at the single-exciton level overcome the large damping of the plasmon mode. Here, we demonstrate that these two hindrances can be overcome by attaching individual J aggregates to single cuboid Au@Ag nanorods. In such hybrid nanosystems, both the ultrasmall mode volume of ~ 71 nm^3 and the ultrashort interaction distance of less than 0.9 nm make the coupling coefficient between a single J-aggregate exciton and the cuboid nanorod as high as ~ 41.6 meV, enabling strong light-matter interactions to be achieved at the quantum optics limit in single open plasmonic nanocavities.

DOI: 10.1103/PhysRevLett.118.237401

Strong light-matter interactions not only are significant from a fundamental quantum optics point of view [1–6], but also are beneficial for exploring advanced quantum devices. These interactions enable light control at the single-photon level, giving rise to novel, advanced applications, such as ultrafast single-photon switches [7,8], single-atom lasers [9], quantum networks [10,11], and quantum information processing [12–14]. These phenomena are rooted in the strong coupling of single quantum emitters to single-mode fields via the coherent exchange of energy between the two subsystems on time scales faster than their dissipative dynamics processes, which manifests itself as mode hybridization and vacuum Rabi splitting in the frequency domain [1,15].

Generally, two types of systems are employed to realize strong light-matter interactions: traditional cavity quantum electrodynamics systems including various optical microcavities [2–5,16–18], which have been widely explored at cryogenic temperatures and in ultrahigh vacuums, and plasmonic nanocavity systems [19–28], which possess the merits of achieving strong light-matter interactions at room temperature and not requiring closed cavities [24]. In addition, such systems are considered to be ideal building blocks for integrating ultrasmall, broad-bandwidth quantum devices [1,29]. Although strong light-matter interactions have been recently achieved at the single-emitter level in closed plasmonic nanocavities [16,17], they have not yet been realized in single open plasmonic nanocavities (Table S1 [30]). To date, the minimum number of excitons that has been strongly coupled to the single open plasmonic nanocavity of a Ag nanoprism is $\sim$70–85, but this is still rather far from the quantum optics limit [1,24].

Two challenges have severely hindered the realization of the strong-coupling limit. One challenge is the precise integration of single-exciton emitters with open plasmonic nanostructures. The other is ensuring that the coupling strength between these components overcomes the large dissipation of the plasmon mode. To overcome these challenges, we first developed a full quantum approach to describe the plasmon-exciton coupling and to determine the specific strong-coupling condition at the quantum optics limit. We then followed this approach to design our experiments precisely and to achieve strong light-matter interactions in single open plasmonic nanocavities at the single-exciton level.

For a system of N quantum emitters strongly interacting with a single metallic nanoparticle, the extinction spectrum of the strongly coupled system is given by (Sec. S1 [30])

$$\sigma(\omega) \propto -\mathrm{Im}\left(\hbar\omega - \varepsilon_d + \delta\omega_d + i\frac{\Gamma_d}{2} - \frac{(\sqrt{N}g_{dc})^2(1-2n_c)}{\hbar\omega - \varepsilon_c + (1-2n_c)(\delta\omega_c + i\frac{\Gamma_c}{2})}\right)^{-1}, \quad (1)$$

where $\varepsilon_d = \hbar\omega_d$ and $\varepsilon_c = \hbar\omega_c$ are the energies of the plasmon mode and emitter fermion, respectively; $\Gamma_d = \hbar\kappa$ is the decay rate of the plasmons; $\Gamma_c = \hbar\gamma_0$ is the resonant width of the emitter; and $\delta\omega_d$ and $\delta\omega_c$ represent frequency shifts. In Eq. (1), g_{dc} is the coupling coefficient between a single emitter and the plasmon mode [31] and is given by

$$g_{dc} = \frac{\hbar\omega_c}{\sqrt{2\hbar\varepsilon_0\omega_d V_{\text{eff}}}}\boldsymbol{\mu}_c \cdot \hat{\boldsymbol{f}}_d(\boldsymbol{r}_c), \tag{2}$$

where $V_{\text{eff}} = V_m \times n^2(\boldsymbol{r})$ is the effective mode volume of the plasmon mode; V_m is the actual mode volume; $n(\boldsymbol{r})$ is the refractive index at $\boldsymbol{r}$; $\boldsymbol{\mu}_c$ and $\boldsymbol{r}_c$ are the dipole moment and location of the emitter, respectively; and $\hat{\boldsymbol{f}}_d(\boldsymbol{r}) = \boldsymbol{E}_d(\boldsymbol{r})/|\boldsymbol{E}_d(\boldsymbol{r})|_{\max}$ is the normalized electric field (EF) of the plasmon mode. Assuming that the system is initially in the ground state, so that $n_c = \langle c^+ c\rangle = 0$, the hybrid mode energies of the strongly coupled system can be derived from Eq. (1) as (Sec. S1 [30])

$$\varepsilon_\pm = \varepsilon_c + \frac{\Delta}{2} \pm \frac{1}{2}\sqrt{4Ng_{dc}^2 + \left(\Delta + i\frac{\Gamma_d - \Gamma_c}{2}\right)^2} - i\frac{\Gamma_d + \Gamma_c}{4}, \tag{3}$$

where $\Delta = \varepsilon_d - \varepsilon_c$ is the detuning. At resonance, Eq. (3) gives the theoretical Rabi splitting criterion $Ng_{dc}^2 > (\Gamma_d - \Gamma_c)^2/16$. Apparently, since the splitting levels $\varepsilon_\pm$ are damped modes with linewidths characterized by $(\Gamma_d + \Gamma_c)/2$, the actual Rabi splitting will be clearly visible only if the splitting gap ($\hbar\Omega_R = \varepsilon_+ - \varepsilon_-$) is bigger than the widths of the new modes, making the observable Rabi splitting condition become $Ng_{dc}^2 \geq (\Gamma_d^2 + \Gamma_c^2)/8$ and the quantum optics limit condition for a single emitter be given by $g_{dc}^2 \geq (\Gamma_d^2 + \Gamma_c^2)/8$. This condition requires g_{dc} to be as large as possible and Γ_d and Γ_c to be as small as possible. As discussed above, a large μ_c, an ultrasmall V_m, and a short interaction distance between the emitter and the metallic nanoparticle can result in a large g_{dc}. Following these theoretical guidelines, we fabricated a cuboid metallic nanorod (NR) with an ultrasmall V_m to support strong coupling at the quantum optics limit.

Since plasmonic nanostructures with sharp tips facilitate the reduction of V_m for the plasmon mode [27], we utilized Ag nanoshells to coat Au NRs (Sec. S2, Fig. S1 [30]) and to construct Au@Ag NR cuboids. With increasing shell thickness, the NR shape gradually changes from a capsule to a cuboid [Fig. 1(a) and Fig. S2 [30]]. Figure 1(b) shows that the EFs sustained by the cuboid Au@Ag NRs are highly localized around their sharp corners, dramatically reducing the V_m of the NRs. Further calculations (Sec. S3 [30]) revealed that V_m decreased from ~6585 nm^3 for the capsule Au NR to ~71 nm^3 for the cuboid Au@Au NR with slightly rounded corners, representing a reduction by ~93 times (Table S2 [30]). Such ultrasmall V_m are associated with the highly localized EFs sustained by the cuboid NRs. Figure 1(c) shows that the EF localization sensitively depends on the NR shape. As the NR shape changes from a capsule to a cuboid, the EF is highly squeezed into a region of ~1 nm around each corner, causing g_{dc} to decrease drastically as the emitter distance from the vertices of the corners increases (Table S3 [30]). Moreover, by precisely controlling the Ag-shell thickness,

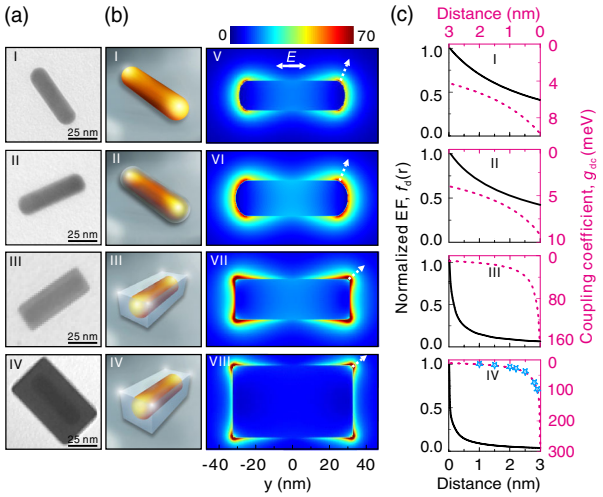

FIG. 1. (a) Transmission electron microscopy (TEM) images of (I) a Au NR and (II)–(IV) Au@Ag NRs with capsule and cuboid shapes. (b) Left: (I)–(IV) Schematic views of the NRs shown in (a). Right: Finite-difference time-domain (FDTD) simulated EF distributions of the LLSPR mode supported by (V) the Au NR (length, 58 nm; diameter, 16 nm) and Au@Ag NRs modeled as (VI) a capsule with a 1.5 nm Ag nanoshell and (VII),(VIII) cuboids with Ag nanoshells of 2 and 4 nm in length and 3 and 11.5 nm in width, respectively. The cuboid NRs have eight slightly rounded corners (the curvature radius at each corner is 1 nm). (c) Normalized EF f_d (**r**) and g_{dc} as functions of the emitter distance from the vertex of the corner along the direction of the maximum EF [dashed white arrows in (b)]. The dashed pink lines and blue stars are the g_{dc} obtained from Eq. (2) and using *ab initio* calculations, respectively. μ_c was set to 0.7 e nm.

the longitudinal localized surface plasmon resonance (LLSPR) wavelength λ_{LLSPR} of the NR can be simultaneously tuned with an accuracy of ~5 nm [Fig. S3(d) [30]], approaching the theoretical accuracy of ~4 nm (Sec. S4, Fig. S4 [30]). This fine-tuning is beneficial for realizing resonant Rabi splitting, which originates from the high sensitivity of the LLSPR modes to the aspect ratios (Fig. S5 [30]), and precise Ag-shell thickness control.

According to the above calculations, to realize strong coupling between a single exciton and a cuboid Au@Ag NR, the interaction distance between them must be less than 1 nm. Thus, we fabricated ultrathin, ~1-nm-thick J aggregates to integrate with the cuboid NRs. When a monolayer of J aggregates was assembled on a cuboid NR, the average interaction distance between the J-aggregate exciton and the NR was ~0.5 nm, yielding $g_{dc} \sim 41.6$ meV based on $\mu_c \sim 0.7$ e nm determined for a single J-aggregate exciton (Sec. S3, Fig. S3 [30]). To confirm this value, we calculated g_{dc} using *ab initio* calculations [32] and found the g_{dc} obtained via the two methods to be highly consistent [Fig. 1(c) IV and Table S3 [30]]. The high localization of the EFs around the vertices also indicates that only one exciton in the nearest J-aggregate chain may be involved in strong coupling at each corner, because the distance of the excitons in the

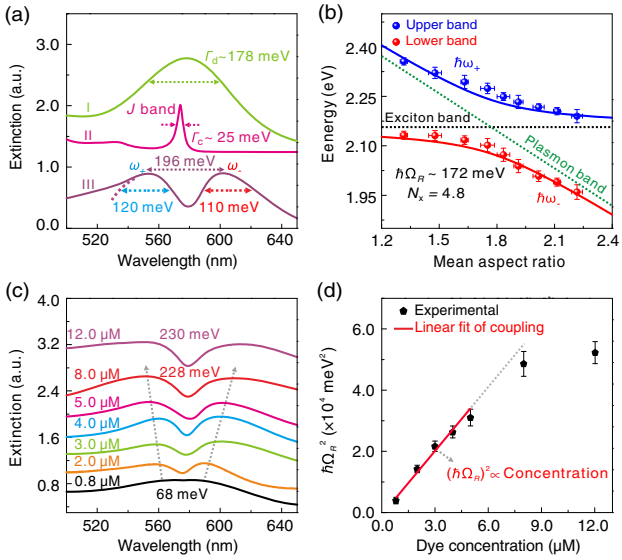

FIG. 2. (a) Extinction spectra of (I) bare Au@Ag NRs, (II) pristine (PIC) J aggregates, and (III) Au@Ag NR/J-aggregate ensembles. (b) Dispersions of the hybrid states extracted from the experimental data (blue and red dots) and calculated using Eq. (3) (blue and red lines). In the calculations, $N_x = 4.8$, $\bar{\Gamma}_d \sim 164$ meV (a mean value for the Au@Ag NR ensembles with different MARs), $\Gamma_c \sim 25$ meV, and $g_{dc} \sim 41.6$ meV were used. The dashed black and green lines represent the uncoupled exciton and LLSPR energies, respectively. The ensembles were treated with 5.0 μM dye solution. (c) Typical extinction spectra of the Au@Ag NRs with $\lambda_{\mathrm{LLSPR}} = 575 \pm 5$ nm strongly coupled to J aggregates and treated with 0.8–12.0 μM dye solutions. The individual curves are offset vertically for clarity. (d) $(\hbar\Omega_R)^2$ as a function of the dye concentration. The red line is the linear fit of $(\hbar\Omega_R)^2$ for the samples treated with 0.8–5.0 μM dye solutions. The error bars in (b) and (d) represent the standard deviations calculated from the three extinction spectra measured in each case.

next-nearest J-aggregate chains to the NR is greater than ~1.5 nm, causing a drastic decrease of g_{dc} (Table S3 [30]). Therefore, for a hybrid nanosystem consisting of a single cuboid NR and J aggregates, the number of J-aggregate excitons participating in strong coupling does not exceed eight, which will lead to Rabi splitting saturation.

The extinction properties of the (PIC) J aggregates and cuboid Au@Ag NRs in which the LLSPR mode is resonant with the J-aggregate transition, as well as the schematics of their hybrids, are depicted in Fig. S3. The combination of J aggregates and the cuboid NRs provides opportunities to observe new optical phenomena based on strong plasmon-exciton coupling. Figure 2(a) presents the extinction spectra of the bare Au@Ag NRs, (PIC) J aggregates, and strongly coupled Au@Ag NR/J aggregates in solutions. When the cuboid Au@Ag NRs supporting LLSPR modes matching the J band (~575 nm) are hybridized with the molecular aggregates, the strongly coupled hybrids exhibit significant mode splitting (~196 meV) into upper (ω_+) and lower (ω_-) plasmon-exciton polariton branches that are part light and part matter (Sec. S5, Fig. S6 [30]) [33,34]. Figure 2(b) demonstrates that, as the mean aspect ratios (MARs) of the NRs are changed to make λ_{LLSPR} vary across the J band (Fig. S7 [30]), the extinction spectra split into two polariton branches exhibiting remarkable anticrossing behavior (Fig. S8 [30]) with Rabi splitting $\hbar\Omega_R$ of ~172 meV.

According to Eq. (3), the square of the Rabi splitting $(\hbar\Omega_R)^2$ is proportional to the number N_x of J-aggregate excitons involved in strong couplings as

$$(\hbar\Omega_R)^2 = 4g_{dc}^2 N_x - \frac{(\Gamma_d - \Gamma_c)^2}{4}, \tag{4}$$

which is confirmed by Figs. 2(c) and 2(d). When the number of Au@Ag NRs was left unchanged but the number of J aggregates assembled on each Au@Ag NR was varied (Sec. S6, Figs. S9 and S10 [30]), $\hbar\Omega_R$ ranging from ~68 to 230 meV were obtained [Fig. 2(c)]. For the hybrid NR ensembles prepared by treating Au@Ag NRs with dye solutions ranging from 0.8 to 5.0 μM, $(\hbar\Omega_R)^2$ and the dye concentration closely follow a linear relationship [Fig. 2(d)], just as Eq. (4) predicts. However, as the dye concentration increases from 0.8 to 12.0 μM, $(\hbar\Omega_R)^2$ increases only slightly from $\sim(4.9 \pm 0.40) \times 10^4$ to $(5.2 \pm 0.36) \times 10^4$ meV^2 [Fig. 2(d)], confirming that Rabi splitting saturation occurs in Au@Ag NR/J aggregates.

To observe strong light-matter interactions in single Au@Ag NR/J aggregates, dark-field scattering measurements were performed (Sec. S7, Fig. S11 [30]). Figure 3(a) shows the scattering spectra of a bare Au@Ag NR and the same NR strongly coupled to J-aggregate excitons, yielding $\hbar\Omega_R \sim 181$ meV. By considering the experimental values of $\Gamma_d \sim 120$ meV and $\Gamma_c \sim 25$ meV, this splitting satisfies the strong-coupling criterion $\hbar\Omega_R > (\Gamma_d + \Gamma_c)/2$. Figure 3(b) presents the scattering spectra of three individual Au@Ag NR/J-aggregate hybrids with different detunings and, therefore, different colors. The LLSPR-exciton couplings in different single hybrids with various detunings can be found in Fig. S12. Figure 3(c) I demonstrates the normalized scattering spectra for different individual hybrids ordered according to detuning, in which anticrossing behavior with $\hbar\Omega_R \sim 108$ meV is clearly observable, indicating that the strong-coupling regime is reached [35]. Figure 3(c) II shows the extinction spectra for $\bar{N}_x = 1.7$ that were calculated using Eq. (1), in which g_{dc} was set to a mean value of $\bar{g}_{dc} \sim 41.3$ meV (Sec. S8, Fig. S13 [30]) and the rest of the parameters were extracted from the experimental results [Fig. 3(a) and Fig. S14 [30]]. The calculated results agree well with the experimental measurements, and such consistency can also be found in the strong-coupling case with $\hbar\Omega_R \sim 179$ meV [Fig. 3(d) I]. In this case, the mean number $\bar{N}_x$ was calculated to be 4.6. In addition, further evidence of strong coupling in these investigated hybrid NRs can be observed as spectral dips in calculated single-hybrid-NR absorption spectra [25] (Fig. S15 [30]), despite such measurements being still unavailable (Fig. S16 [30]).

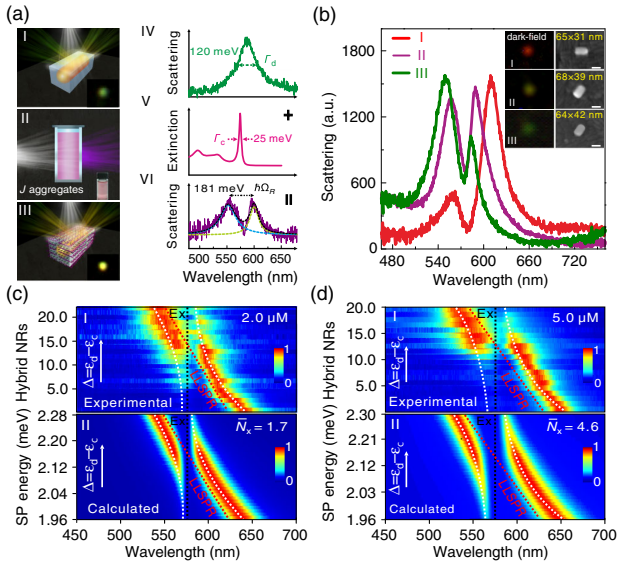

FIG. 3. (a) Left: Schematics of the optical measurements for (I) a bare Au@Ag NR, (II) J aggregates, and (III) a strongly coupled Au@Ag NR/J-aggregate hybrid. The insets are dark-field images of the individual NRs and a photograph of the J-aggregate solution in the reaction vessel used for the measurements. Right: (IV)–(VI) Spectra obtained by performing the measurements as shown in the left panel. The dashed lines represent the Lorenz-fitted results. (b) Scattering spectra of three individual Au@Ag NR/J-aggregate hybrids with different detunings ($\Delta < 0$, $\Delta = 0$, and $\Delta > 0$). The insets are dark-field and SEM images of the corresponding hybrid NRs. The scale bar is 50 nm. (c),(d) (I) Scattering spectra of the individual Au@Ag NR/J aggregates ordered according to detuning for the ensembles treated with (c) 2.0 and (d) 5.0 μM PIC dye solutions. (II) Extinction spectra calculated for (c) $\bar{N}_x = 1.7$ and (d) $\bar{N}_x = 4.6$ using Eq. (1). In the calculations, $\bar{\Gamma}_d \sim 135$ meV (a mean value for the bare Au@Ag NRs, Fig. S14 [30]), $\Gamma_c \sim 25$ meV, and $\bar{g}_{dc} \sim 41.3$ meV were used. The dashed black and pink lines represent the uncoupled exciton transition and LLSPR wavelengths, respectively.

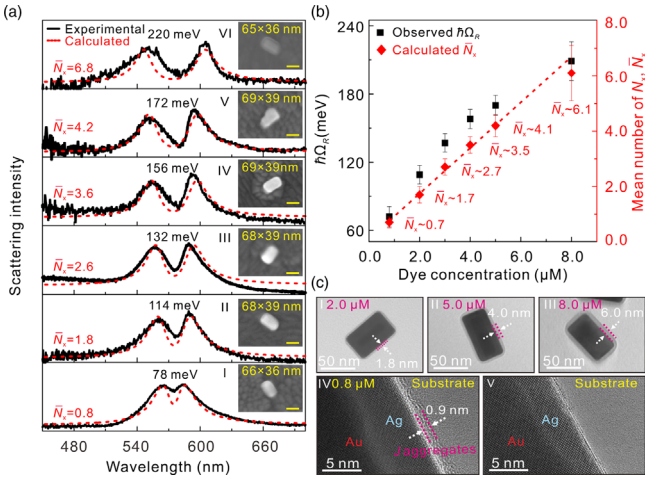

FIG. 4. (a) Black lines: Representative scattering spectra of the individual hybrid Au@Ag NR/J aggregates with different $\hbar\Omega_R$. The individual hybrids (I)–(VI) were isolated from the ensembles treated with 0.8, 2.0, 3.0, 4.0, 5.0, and 0.8 μM dye solutions. Dashed red lines are extinction spectra of the strongly coupled hybrids calculated using Eq. (1). The insets are SEM images of the corresponding hybrid NRs. The scale bar is 50 nm. (b) Statistics of the $\hbar\Omega_R$ measured for individual hybrid NRs and the corresponding $\bar{N}_x$ calculated using Eq. (1) for each dye concentration. About 20–30 hybrid NRs were counted in each case (Fig. S18 [30]). In the calculations, $\bar{g}_{dc} \sim 41.3$ meV, $\bar{\Gamma}_d \sim 135$ meV (the mean value for the bare Au@Ag NRs, Fig. S14 [30]), and $\Gamma_c \sim 25$ meV were used. The dashed red line is a linear fit of $\bar{N}_x$ corresponding to the various dye concentrations. (c) (I)–(III) TEM images of Au@Ag NR/J aggregates with different dye layer thicknesses and (IV),(V) high-resolution TEM (HRTEM) images of the edges of a single Au@Ag NR/J-aggregate hybrid and a bare Au@Ag NR, respectively.

Figure 4(a) shows the representative scattering spectra at resonance for the individual hybrid NRs with different numbers of J aggregates, where the J-aggregate numbers were tailored by treating the Au@Ag NRs with 0.8–8.0 μM PIC dye solutions. The scattering spectra exhibit $\hbar\Omega_R$ ranging from ~78 to 220 meV, which are consistent with those calculated using Eq. (1), where $\bar{g}_{dc} \sim 41.3$ meV, and the corresponding $\bar{N}_x = 0.8$–6.8 are determined. Figure 4(b) presents the statistics of the measured $\hbar\Omega_R$ and calculated $\bar{N}_x$ for single hybrid NRs treated with dye solutions in different concentrations. The calculated spectra agreeing well with the experimental ones confirms that $\bar{N}_x$ ranges from $\sim 0.7 \pm 0.2$ to 6.1 ± 1.0, corresponding to the observed $\hbar\Omega_R$ of $\sim 72 \pm 9.0$–209 ± 17.0 meV [Fig. 4(b) and Fig. S18 [30]]. Furthermore, even considering the nonradiation broadening effects of the energy levels ($\Gamma_d \sim 135$ meV and $\Gamma_c \sim 25$ meV), the strong-coupling condition can be satisfied when $N_x = 1.38$. These results indicate that we achieved strong light-matter interactions at the single-exciton level in single open plasmonic nanocavities.

The realization of strong coupling at the quantum optics limit is further validated by the microscopy images. By precisely controlling the dye concentration and number of Au@Ag NRs, very thin, ~0.9–6.0-nm-thick J-aggregate layers were formed on the NRs [Fig. 4(c) and Fig. S17 [30]]. Since the volume of a single dye monomer is ~0.5 nm^3 [24], when a J aggregate is considered to be a one-dimensional chain of monomers [36], the thickness of a single J-aggregate chain can be estimated to be ~0.8 nm. The ultrathin, ~0.9-nm-thick J-aggregate layer observable in Fig. 4(c) IV suggests that individual J aggregates were successfully assembled on the Au@Ag NR, ensuring that a single J-aggregate exciton was located at a sharp corner of the cuboid Au@Ag NR and that the interaction distance between them was less than 0.9 nm. Such an ultrashort interaction distance ensures a fully spatial overlap between the two subsystems, which facilitates the achievement of strong light-matter interactions in single Au@Ag NR/J aggregates at the quantum optics limit.

In summary, we demonstrated strong light-matter interactions at the quantum optics limit in single open plasmonic

nanocavities with ultrasmall V_m. This work opens up possibilities to remove the ambiguities in explaining the plasmon-exciton couplings, which from the quantum optics perspective translates into uncertainty in the number of excitons involved in strong coupling as well as into a question of whether plasmonic nanocavities are at all capable of realizing strong light-matter interactions at its fundamental limit [24]. These issues are also significant for potential quantum optics applications involving single excitons [5,16,37]. The ability to reach the quantum optics limit of strong light-matter interactions in single open plasmonic nanocavities not only is significant for advancement in the fundamental sciences, but also will promote the development of room-temperature quantum devices.

We thank Dr. J. M. Liu and Dr. H. X. Jiang for their assistance with the data processing and discussions and Professor J. Chen, Mrs. Y. Y. Li, and Dr. R. Zhan for helping with the TEM and HRTEM measurements. This work was supported by the Ministry of Science and Technology of China (Grant No. 2016YFA0301300), the National Natural Science Foundations of China (Grants No. 11334015, No. 11364001, No. 11504050 and No. 61675237), the Natural Science Foundations of Guangdong (Grants No. 2016A030312012 and No. 2014A030313140), and the Guangzhou Science and Technology Projects (Grant No. 201607020023).

R. M. L., Z. K. Z., and Y. C. Y. contributed equally to this work.

*Corresponding author.
wangxueh@mail.sysu.edu.cn

[1] P. Törmä and W. L. Barnes, Rep. Prog. Phys. **78**, 013901 (2015).
[2] T. Yoshie, A. Scherer, J. Hendrickson, G. Khitrova, H. M. Gibbs, G. Rupper, C. Ell, O. B. Shchekin, and D. G. Deppe, Nature (London) **432**, 200 (2004).
[3] R. Bose, T. Cai, K. R. Choudhury, G. S. Solomon, and E. Waks, Nat. Photonics **8**, 858 (2014).
[4] M. Nomura, N. Kumagai, S. Iwamoto, Y. Ota, and Y. Arakawa, Nat. Phys. **6**, 279 (2010).
[5] A. Faraon, I. Fushman, D. Englund, N. Stoltz, P. Petroff, and J. Vučković, Nat. Phys. **4**, 859 (2008).
[6] A. Dousse, J. Suffczyński, A. Beveratos, O. Krebs, A. Lemaître, I. Sagnes, J. Bloch, P. Voisin, and P. Senellart, Nature (London) **466**, 217 (2010).
[7] T. Volz, A. Reinhard, M. Winger, A. Badolato, K. J. Hennessy, E. L. Hu, and A. Imamoğlu, Nat. Photonics **6**, 605 (2012).
[8] W. Chen, K. M. Beck, R. Bücker, M. Gullans, M. D. Lukin, H. T. Suzuki, and V. Vuletić, Science **341**, 768 (2013).
[9] J. McKeever, A. Boca, A. D. Boozer, J. R. Buck, and H. J. Kimble, Nature (London) **425**, 268 (2003).
[10] T. G. Tiecke, J. D. Thompson, N. P. de Leon, L. R. Liu, V. Vuletić, and M. D. Lukin, Nature (London) **508**, 241 (2014).
[11] H. Kim, R. Bose, T. C. Shen, G. S. Solomon, and E. A. Waks, Nat. Photonics **7**, 373 (2013).
[12] A. Wallraff, D. I. Schuster, A. Blais, L. Frunzio, R.-S. Huang, J. Majer, S. Kumar, S. M. Girvin, and R. J. Schoelkopf, Nature (London) **431**, 162 (2004).
[13] T. M. Babinec, B. J. M. Hausmann, M. Khan, Y. Zhang, J. R. Maze, P. R. Hemmer, and M. Lončar, Nat. Nanotechnol. **5**, 195 (2010).
[14] M. J. Holmes, K. Choi, S. Kako, M. Arita, and Y. Arakawa, Nano Lett. **14**, 982 (2014).
[15] K. Hennessy, A. Badolato, M. Winger, D. Gerace, M. Atatüre, S. Gulde1, S. Fält1, E. L. Hu, and A. Imamoğlu, Nature (London) **445**, 896 (2007).
[16] H. Mabuchi and A. C. Doherty, Science **298**, 1372 (2002).
[17] J. P. Reithmaier, G. Sęk, A. Löffler, C. Hofmann, S. Kuhn, S. Reitzenstein, L. V. Keldysh, V. D. Kulakovskii, T. L. Reinecke, and A. Forchel, Nature (London) **432**, 197 (2004).
[18] J. D. Thompson, T. G. Tiecke, N. P. de Leon, J. Feist, A. V. Akimov, M. Gullans, A. S. Zibrov, V. Vuletić, and M. D. Lukin, Science **340**, 1202 (2013).
[19] R. Chikkaraddy, B. de Nijs, F. Benz, S. J. Barrow, O. A. Scherman, E. Rosta, A. Demetriadou, P. Fox, O. Hess, and J. J. Baumberg, Nature (London) **535**, 127 (2016).
[20] K. Santhosh, O. Bitton, L. Chuntonov, and G. Haran, Nat. Commun. **7**, ncomms11823 (2016).
[21] A. E. Schlather, N. Large, A. S. Urban, P. Nordlander, and N. J. Halas, Nano Lett. **13**, 3281 (2013).
[22] J. Bellessa, C. Bonnand, J. C. Plenet, and J. Mugnier, Phys. Rev. Lett. **93**, 036404 (2004).
[23] J. Dintinger, S. Klein, F. Bustos, W. L. Barnes, and T. W. Ebbesen, Phys. Rev. B **71**, 035424 (2005).
[24] G. Zengin, M. Wersäll, S. Nilsson, T. J. Antosiewicz, M. Käll, and T. Shegai, Phys. Rev. Lett. **114**, 157401 (2015).
[25] G. Zengin, G. Johansson, P. Johansson, T. J. Antosiewicz, M. Käll, and T. Shegai, Sci. Rep. **3**, 3074 (2013).
[26] P. Vasa, W. Wang, R. Pomraenke, M. Lammers, M. Maiuri, C. Manzoni, G. Cerullo, and C. Lienau, Nat. Photonics **7**, 128 (2013).
[27] S. D'Agostino, F. Alpeggiani, and L. C. Andreani, Opt. Express **21**, 27602 (2013).
[28] J. Ren, Y. Gu, D. Zhao, F. Zhang, T. Zhang, and Q. Gong, Phys. Rev. Lett. **118**, 073604 (2017).
[29] M. S. Tame, K. R. McEnery, Ş. K. Özdemir, J. Lee, S. A. Maier, and M. S. Kim, Nat. Phys. **9**, 329 (2013).
[30] See Supplemental Material at http://link.aps.org/supplemental/10.1103/PhysRevLett.118.237401 for detailed theory modeling, numerical calculations, experimental materials and methods, SEM and dark-field scattering measurements of Au@Ag/J aggregates, etc., Figs. S1–S18, Tables S1–S4, and Refs. [31–39].
[31] X.-H. Wang, R. Wang, B.-Y. Gu, and G.-Z. Yang, Phys. Rev. Lett. **88**, 093902 (2002).
[32] G. Chen, Y.-C. Yu, X.-L. Zhuo, Y.-G. Huang, H. Jiang, J.-F. Liu, C.-J. Jin, and X.-H. Wang, Phys. Rev. B **87**, 195138 (2013).
[33] L. Shi, T. K. Hakala, H. T. Rekola, J.-P. Martikainen, R. J. Moerland, and P. Törmä, Phys. Rev. Lett. **112**, 153002 (2014).
[34] Y. Sugawara, T. A. Kelf, J. J. Baumberg, M. E. Abdelsalam, and P. N. Bartlett, Phys. Rev. Lett. **97**, 266808 (2006).

[35] T. K. Hakala, J. J. Toppari, A. Kuzyk, M. Pettersson, H. Tikkanen, H. Kunttu, and P. Törmä, Phys. Rev. Lett. **103**, 053602 (2009).
[36] M. Van Burgel, D. A. Wiersma, and K. Duppen, J. Chem. Phys. **102**, 20 (1995).
[37] S. Gröblacher, T. Paterek, R. Kaltenbaek, Č. Brukner, M. Zukowski, M. Aspelmeyer, and A. Zeilinger, Nature (London) **446**, 871 (2007).
[38] A. Manjavacas, F. J. García de Abajo, and P. Nordlander, Nano Lett. **11**, 2318 (2011).
[39] D. N. Zubarev, Sov. Phys. Usp. **3**, 320 (1960).
[40] J. Duan, K. Park, R. I. MacCuspie, R. A. Vaia, and R. Pachter, J. Phys. Chem. C **113**, 15524 (2009).
[41] M. N. O'Brien, M. R. Jones, K. A. Brown, and C. A. Mirkin, J. Am. Chem. Soc. **136**, 7603 (2014).
[42] R. Liu, J.-H. Zhou, Z.-K. Zhou, X. Jiang, J. Liu, G. Liu, and X.-H. Wang, Nanoscale **6**, 13145 (2014).
[43] P. T. Kristensen, C. Van Vlack, and S. Hughes, Opt. Lett. **37**, 1649 (2012).
[44] R. C. Hilborn, Am. J. Phys. **50**, 982 (1982).
[45] D. Melnikau, D. Savateeva, A. Chuvilin, R. Hillenbrand, and Y. P. Rakovich, Opt. Express **19**, 22280 (2011).
[46] A. Benz, S. Campione, S. Liu, I. Montaño, J. F. Klem, A. Allerman, J. R. Wendt, M. B. Sinclair, F. Capolino, and I. Brener, Nat. Commun. **4**, 2882 (2013).